https://doi.org/10.5194/egusphere-2024-434
Preprint. Discussion started: 27 February 2024

CHARACTERIZATION OF THE PARTICLE SIZE DISTRIBUTION, MINERALOGY AND FE MODE OF OCCURRENCE OF DUST-EMITTING SEDIMENTS ACROSS THE MOJAVE DESERT, CALIFORNIA, USA

Adolfo González-Romero[1,2,3], Cristina González-Flórez[1,3], Agnesh Panta[4], Jesús Yus-Díez[5], Patricia Córdoba[2], Andres Alastuey[2], Natalia Moreno[2], Melani Hernández-Chiriboga[1], Konrad Kandler[4], Martina Klose[6], Roger N. Clark[7], Bethany L. Ehlmann[8], Rebecca N. Greenberger[8], Abigail M. Keebler[8], Phil Brodrick[9], Robert Green[9], Paul Ginoux[10], Xavier Querol[2], Carlos Pérez García-Pando[1,11]

[1] Barcelona Supercomputing Center (BSC), Barcelona, Spain
[2] Spanish Research Council, Institute of Environmental Assessment and water Research (IDAEA-CSIC), Barcelona, Spain
[3] Polytechnical University of Catalonia (UPC), Barcelona, Spain
[4] Institute of Applied Geosciences, Technical University Darmstadt, Darmstadt, Germany
[5] Centre for Atmospheric Research, University of Nova Gorica, Ajdovščina, Slovenia.
[6] Karlsruhe Institute of Technology (KIT), Institute of Meteorology and Climate Research Troposphere Research (IMKTRO), Karlsruhe, Germany
[7] PSI Planetary Science Institute, Tucson, AZ, USA
[8] California Institute of Technology, Division of Geological and Planetary Sciences, Pasadena, CA, USA
[9] Jet Propulsion Laboratory, California Institute of Technology
[10] NOAA Geophysical Fluid Dynamics Laboratory, Princeton, NJ, USA
[11] Catalan Institution for Research and Advanced Studies (ICREA), Barcelona, Spain

Corresponding author: Adolfo González-Romero (agonzal3@bsc.es) and Xavier Querol (xavier.querol@idaea.csic.es)

https://doi.org/10.5194/egusphere-2024-434
Preprint. Discussion started: 27 February 2024

Abstract

Understanding the effect of dust upon climate and ecosystems needs comprehensive analyses of the physiochemical properties of dust-emitting sediments in arid regions. Here, we analyse a diverse set of crusts and aeolian ripples (n=55) from various dust-hotspots within the Mojave Desert, California, USA, with focus on their particle size distribution (PSD), mineralogy, aggregation/cohesion state and iron mode of occurrence characterization. Our results showed differences in fully and minimally dispersed PSDs, with crusts average median diameters (92 and 37 µm, respectively) compared to aeolian ripples (226 and 213 µm, respectively). Mineralogical analyses unveiled variations between crusts and ripples, with crusts enriched in phyllosilicates (24 vs 7.8 %), carbonates (6.6 vs 1.1 %), Na-salts (7.3 vs 1.1 %) and zeolites (1.2 and 0.12 %), while ripples enriched in feldspars (48 vs 37 %), quartz (32 vs 16 %), and gypsum (4.7 vs 3.1 %). Bulk Fe content analyses indicate higher concentrations in crusts (3.0±1.3 wt %) compared to ripples (1.9±1.1 wt %), with similar Fe speciation proportions; nano Fe-oxides/readily exchangeable Fe represent ~1.6 %, hematite/goethite ~15 %, magnetite/maghemite ~2.0 % and structural Fe in silicates ~80 % of the total Fe. We identified segregation patterns in PSD and mineralogy differences within the Mojave basins, influenced by sediment transportation dynamics and precipitates due to groundwater table fluctuations. Mojave Desert crusts show similarities with previously sampled crusts in the Moroccan Sahara for PSD and readily exchangeable Fe, yet exhibit differences in mineralogical composition, which could influence the emitted dust particles characteristics.

Keywords: Arid regions, dust sources, desert dust, dust-emitting sediment formation model, dust mineralogy.

https://doi.org/10.5194/egusphere-2024-434
Preprint. Discussion started: 27 February 2024

1. Introduction

Desert dust produced by wind erosion of arid and semi-arid surfaces has important effects on climate and ecosystems (Weaver et al., 2002; Goudie & Middleton, 2006; Sullivan et al., 2007; Crumeyrolle et al., 2008; De Longeville et al., 2010; Karanasiou et al., 2012; Pérez García-Pando et al., 2014; among others). Dust affects the energy and water cycles through its absorption and scattering of both shortwave (SW) and longwave (LW) radiation (Perez et al., 2006; Miller et al., 2014), and exerts influence on cloud formation, precipitation patterns, and the associated indirect radiative forcing by serving as nuclei for liquid and ice clouds (Harrison et al., 2019). Dust also undergoes heterogeneous chemical reactions in the atmosphere that enhance their hygroscopicity and modify their optical properties (Bauer et al., 2005), and when deposited into ocean waters, its bioavailable iron content acts as a catalyst for photosynthesis by ocean phytoplankton, thereby increasing carbon dioxide uptake and influencing the global carbon cycle (Jickells et al., 2005).

Both dust emission processes and climate perturbations by dust depend fundamentally upon the physical and chemical properties of the dust-emitting sediments from different sources. For instance, the particle size distribution (PSD) and cohesion of the sediments affect saltation bombardment and aggregate disintegration processes involved in dust emission (Shao et al., 1993). The content of iron oxides (mainly hematite and goethite) determines the absorption of solar radiation by dust (Formenti et al., 2014; Engelbrecht et al., 2016; Di Biagio et al., 2019; Zubko et al., 2019), that of nano Fe oxides and easily exchangeable Fe increase the fertilising effect of dust in ocean and terrestrial ecosystems (Baldo et al., 2020), and that of K-feldspar and quartz increases the ice nucleation efficiency of dust (Atkinson et al., 2013; Harrison et al., 2019; Chatziparaschos et al., 2023). Overall, a notable gap exists in our understanding of the properties of dust-emitting sediments, including particle size distribution, cohesion, mineral composition, and Fe mode of occurrence from different dust sources. This deficiency hinders the development of precise model simulations necessary for accurately assessing the emission and transport of dust and its associated climate and environmental impacts (Raupach et al., 1993; Laurent et al., 2008; Perlwitz et al., 2015; Kok et al., 2021).

This study focuses on the characterization of dust-emitting sediments from the Mojave Desert. The Mojave Desert is a closed-basin wedge-shaped region located in the southwestern United States, between California and Nevada. The region is surrounded by mountain ranges and traversed by the Mojave river and other intermittent rivers for over 200 km from the San Bernardino mountains to the east (Dibblee, 1967, Reheis et al., 2012). Despite its limited global importance (dust emission from North America represents only ~3 % of the global dust emission, Kok et al., 2021), the Mojave Desert is an important regional dust source (Ginoux et al., 2012), with most emission occurring in the playa lakes. Reynolds et al. (2009) observed 71 days with dust plumes during 37 months of camera recording at the Franklin playa lake. According to remote sensing data (MODIS) from years 2000-2005 over the Mojave Desert, aerosol optical depth (AOD) is higher in spring and summer and reaches a minimum in winter (Frank et al., 2007). However, from November to May, eastward flows of the jet-stream affect the Mojave Desert, which, in combination with topography, favour the development of northern winds that can lead to dust emission (Urban et al., 2009). Up to 65 % of emission in the Mojave Desert is estimated to be due to natural while the remaining 35 % is caused by anthropogenic activities, including off-road recreation practices, mine operations, and military training, while cattle grazing has reduced vegetation cover (Frank et al., 2007). The AOD in this region is also affected by dust transported from other regions (Tong et al., 2012) and pollution transported from the Los Angeles

https://doi.org/10.5194/egusphere-2024-434
Preprint. Discussion started: 27 February 2024

Basin (Frank et al., 2007, Urban et al., 2009). In the Mojave Desert, Reynolds et al. (2009) noted an association between wet periods and dust emission, directly related to the generation of new thin crusts and salt crust removal.

The Mojave Desert includes several significant playa lakes, such as Rogers and Rosemond, Owens Lake, Death-Valley-Badwater, Panamint Valley, Bristol, Cadiz and Danby, Searles Lake, Soda Lake, and Mesquite Lake, among others (Potter and Coppernoll-Houston, 2019). Reynolds et al. (2009) distinguished between two types of playa lakes: wet playas influenced by groundwater, and dry playas, unaffected by groundwater, though both can experience surface-water runoff. Goudie (2018) further delineated wet playas as having a groundwater table within 5 m of the surface, while dry playas have a groundwater table deeper than 5 m. Additionally, Goudie (2018) observed that the interaction between salt minerals and the groundwater table on wet playas lead to the formation of fluffy surfaces through salt reworking by water during evapotranspiration.

Eghbal & Southard (1993) described three different aridisols present in the Rand mountains alluvial fan. The uppermost layer, ranging from 0 to 1 cm in depth exhibited a texture of 15-30% gravel, 69-74 % sand and 10-11 % clay. The mineralogy of those samples was dominated by quartz, feldspars, amphiboles, and clay minerals, including smectite, mica and kaolinite (Eghbal & Southard, 1993). The Cronese Lakes and Soda Lake playas are documented to contain salt precipitates, but mineralogy is not specified. Mesquite Lake playa is noted for its gypsum deposits (Reynolds et al., 2009). At Franklin Lake playa, surfaces are characterized by silt-clay size particles (Goldstein et al., 2017) with mineralogical descriptions provided by Reynolds et al. (2009) indicating fluffy surfaces comprised of halite, thenardite, trona, burkeite, calcite, illite, smectite, and kaolinite. Furthermore, Goldstein et al. (2017) identified a diverse array of minerals at Franklin Lake playa, including clays, zeolites, plagioclase, K-feldspar, quartz, calcite, dolomite and salt minerals such as trona, halite, burkeite and thenardite.

This study characterises the particle size distribution, mineralogy and mode of occurrence of Fe of dust-emitting sediments in the Mojave Desert, where a sediment sampling was carried out in 2022 around the Soda, Mesquite, Ivanpah, Coyote and Cronese playa lakes, in the context of the FRontiers in dust minerAloGical coMposition and its Effects upoN climate (FRAGMENT) project. The results are compared with those from previous campaigns carried out in the Moroccan Sahara in 2019 (González-Romero et al., 2023) and Iceland in 2021 (González-Romero et al., 2024).

2. Methodology

2.1 Study area

The Mojave Desert, located between California and Nevada, has a diverse geological history spanning from the Cambrian and Precambrian eras to the Holocene. This geological complexity encompasses volcanic, plutonic, metamorphic, and sedimentary units (Jennings et al., 1962; Miller et al., 2014). In areas once submerged during the last glacial maximum, we now find ephemeral playa lakes, offering a glimpse into the region's dynamic past (Miller et al., 2018). These playa lakes, surrounded by a variety of source rocks, exhibit diverse particle sizes and compositions. One such examples is Soda Lake, located near Baker, CA, which undergoes influences from aeolian, alluvial and fluvial processes, and

https://doi.org/10.5194/egusphere-2024-434
Preprint. Discussion started: 27 February 2024

experiences an annual precipitation of 80-100mm (Urban et al., 2018). This ephemeral lake contains salts resulting from the evaporation of groundwater sourced from an aquifer nestled in the Zzyzx mountains (Honke et al., 2019). Dust emissions are a recurrent phenomenon, primarily originated from fine sediments accumulated in the lake´s central areas during sporadic floodings, as well as from the white evaporite surfaces found in the lake (Urban et al., 2018).

Samples of dust-emitting sediments were collected from various sites within the Mojave Desert region. Among these sites is Soda Lake, situated near the Zzyzx complex, which is linked to Silver Lake to the north, and surrounded by igneous, volcanic and carbonate rocks, as well as dune fields to the south (Figure 1). Adjacent to Soda Lake lie the Cronese lakes, positioned to the northwest and sharing a similar geologic context (Figure 1). Mesquite Lake, located on the border between California and Nevada, is encircled by carbonate and igneous rocks, mirroring the geological setting of the nearby Ivanpah Lake (Figure 1). Notably, Mesquite Lake playa is the only playa affected by a gypsum-mine pit, as documented by Reynolds et al. (2009). Further contributing to the diversity of the region's geological makeup is Coyote Lake, flanked by Miocene and Pleistocene sediments (Figure 1). These playa lakes, characterized as endorheic ephemeral lakes, receive in some cases groundwater inputs, enriching the lakes with salts that subsequently precipitate on the surfaces of their central regions (Whitney et al., 2015; Urban et al., 2018).

Figure 2 illustrates the regional distribution of the annual Frequency of Occurrence (FoO) of dust events with dust optical depth exceeding 0.1, as derived from MODIS Deep Blue C6.1 Level 2 data. Notably, the map highlights active dust hotspots at Soda, Cronese, and Coyote lakes, as well as at Ivanpah and Mesquite lakes, alongside other notable areas (Figure 2). Preliminary mineralogical identification maps derived from the Earth Surface Mineral Dust Source Investigation (EMIT) imaging spectrometer onboard of the International Space Station (Green et al., 2020) based on the mineral mapping refinement technique developed by Clark et al. (2023) known as Tetracorder, offer a glimpse into the rich mineralogical tapestry of the region (Figure 3). These analyses reveal the widespread presence of phyllosilicates such as kaolinite, smectite, montmorillonite, and illite across the area, with the northeastern sector, particularly around Mesquite Lake, exhibiting notable concentrations of carbonates and gypsum. Additionally, goethite and hematite are detected, with a more pronounced presence of goethite in the northern portion and of hematite in the southern part of the region. Of significance is the detection of mixtures of Fe^{2+} and Fe^{3+} within various minerals, enriching our understanding of the region's mineralogical diversity.

2.2 Sampling

Representative surfaces of dust-emitting sediments were sampled in the above playa lakes, with depths of up to 3 cm, using a 5 cm^2 inox shovel. Samples were stored in a plastic bag, labelled, and documented with photographs, descriptions, and coordinates, and transported to the laboratories for subsequent analyses. The type of samples considered are crusts (semi-cohesive fine sediments accumulated during floodings in depressions) and ripples (aeolian ripples that are built up under favourable winds and supply sand for saltation) (Figure 4). Once in the laboratory, the samples were dried for 24-48 h at 40-50 ºC, sieved to pass through a 2 mm mesh, and separated into homogeneous sub-samples for subsequent analyses.

https://doi.org/10.5194/egusphere-2024-434
Preprint. Discussion started: 27 February 2024

A total of 55 surface sediments and ripples (32 from Soda Lake, 9 from Mesquite Lake, 1 from Ivanpah Lake, 11 from the Cronese Lakes, and 2 from Coyote Lake) were sampled in May 2022 for laboratory analysis.

2.3 Analyses

2.3.1 Particle size distribution

Particle size distributions (PSD) were analysed as described in González-Romero et al. (2023) to characterise the natural aggregation of particles in the sample in a minimally dispersed condition (MDPSD) as well as following disaggregation to measure the PSD of the sample in a fully dispersed condition (FDPSD). Both PSDs (MDPSD and FDPSD) were obtained by a laser diffractometer with the Malvern Mastersizer 2000 Hydro G and Scirocco for the fully and minimally dispersed conditions, respectively. The method for fully dispersed characterization followed the procedure described by Sperazza et al. (2004).

2.3.2 Mineralogical composition

To quantify the different contents of crystalline minerals and amorphous components, X-Ray Diffraction (XRD) coupled with a Rietveld quantitative method were used (Rietveld, 1969; Cheary and Coelho, 1992; Young, 1995 and Topas, 2018). Adding a known amount of an internal standard material allowed, via the Rietveld method, the quantification of a mixture of minerals and any non-crystalline material in the mixture not included in the Rietveld method (De la Torre et al., 2001; Madsen, 2001, Scarlett and Madsen, 2006; Machiels et al., 2010; Ibañez et al., 2013). For the analysis, a measured amount of dry grounded sample is mixed and dry grounded again with 10-20 % of fluorite (CaF_2 powder, Merck), used here as an internal standard for quantitative purposes. The XRD patterns of the samples were analysed by a Bruker D8 A25 Advanced Powder X-ray diffractometer operated at 40kV and 40 mA with monochromatic Cu Kα radiation (=1,5405 Å). This device uses a Bragg-Brentano geometry and a sensitive detector LynxEye 1D. Diffractograms were recorded from 4 to 120º of 2θ and steps of 0.015º in 1s and maintained rotation (15/min). For the clay identification, samples were analysed using the oriented aggregate method by XRD, decanting clay fractions from samples and smearing the slurries in glass slides. After, three treatments were applied including air drying (AO), glycolation with ethylene glycol (AG) and heating at 550 ºC for 2h (AC) with its three different diffractograms. Finally, the three diffractograms allows us to corroborate the presence of Illite, Chlorite, Palygorskite and Montmorillonite through Thorez (1976) and USGS Open File procedures. Data collected were evaluated using the Bruker AXS DIFFRAC.EVA software package (Bruker AXS, Karlsruhe, Germany, 2000) and the Rietveld analyses performed with TOPAS 4.2 program (Bruker AXS, 2003-2009). A Chebyshev function of level 5 was used to fit the background and abundances of crystalline phases and amorphous phases were normalised to 100 wt %. Fits were evaluated by visual comparison, the R_{wp} (R-weighted pattern), R_{exp} (R-expected), and Goodness of Fit (GOF).

2.3.3 Mode of occurrence of Fe

As XRD is not precise enough for Fe-oxide quantification, wet chemistry and sequential extractions of Fe are needed for quantification of the Fe mode of occurrence (González-Romero et al., 2023; 2024). Samples were analysed with a two-step acid digestion for the total Fe (FeT) content following the

https://doi.org/10.5194/egusphere-2024-434
Preprint. Discussion started: 27 February 2024

procedure by Querol et al. (1993, 1997). A reference material (NIST-1633b, coal fly ash) was used for quality control in every batch. The sequential extraction presented in Shi et al. (2009), Baldo et al. (2020) and González-Romero et al. (2024) was used to quantify readily exchangeable Fe ions and nano Fe oxides (FeA), the amount of crystalline Fe oxides as goethite and hematite (FeD), and crystallised magnetite (FeM). For the 1st extraction, a 30 mg sample was leached with 10 ml of an ascorbate solution (extractant solution) and shaken in dark conditions for 24 h and filtered. Another 30 mg was leached with 10 ml of a dithionite solution (extractant solution), shaken for 2 h in dark conditions and filtered for the 2nd extraction. The solid residue was then leached again in 10 ml of an oxalate solution for 6 h in dark conditions and filtered for the 3rd extraction. The extracted solution of each phase (FeT, FeA, FeD and FeM) was analysed to quantify dissolved Fe by Inductively Coupled Plasma Atomic Emission Spectrometry (ICP-AES). FeA is obtained with the 1st extraction, FeD is obtained subtracting from the 2nd extraction the amount of Fe from the 1st extraction. Finally, the FeM is related to the 3rd extraction. At the end, the equivalent to the Fe as structural Fe was obtained: FeS = FeT - FeA - FeD - FeM which is included in other minerals and amorphous phases. To test accuracy, 30 mg of Arizona Test Dust (ATD; ISO 12103-1, A1 Ultrafine Test Dust; Powder Technology Inc.) was subjected to the same extraction procedure in every batch and extraction.

The averaged Fe content of the reference material 1633b was 7.6 ± 0.5 % (certified 7.8%). Furthermore, the average values of the sequential Fe extraction of the ATD reference material were 0.073 ± 0.012, 0.47 ± 0.01, and 0.042 ± 0.002 % for FeA, FeA+FeD and FeM, respectively, while the certified contents are 0.067, 0.48, and 0.047 %, respectively.

3. Results

3.1. Particle size distribution

The PSD and the median particle diameter are key parameters to understand the cohesion/aggregation state of the sediments (González-Romero et al., 2024). In the case of the Mojave Desert, some basins are enriched in salts, which can cause some artefacts in the FDPSD, as there can be removal of the aggregating agents by dissolution during the wet dispersion for the PSD analysis. These salt cementation of the crusts might yield very reduced dust emissions.

The average PSDs of crusts across different basins exhibit remarkable similarity, yet disparities between FDPSDs and MDPSDs are pronounced, indicating varying degrees of particle cohesion and aggregation at Cronese, Mesquite, Ivanpah and Coyote lakes. In these locations, FDPSDs feature a dominant mode at 8-10 µm alongside a coarser mode at 100 µm, while MDPSDs are characterized by a dominant coarser mode (Figure 5). In contrast, Soda Lake crusts, exhibit similarity between FDPSDs and MDPSDs. When comparing averaged FDPSDs and MDPSDs of aeolian ripples from the Mojave Desert, they are found to be similar, typically featuring a major size mode between 100-300 µm. However, distinctions arise analysing specific lakes. Aeolian ripples from Soda, Cronese, and Coyote lakes showcase a dominant coarse mode at 200-300 µm, while those from Mesquite Lake show a dominant mode at a finer scale, approximately at 100 µm (Figure 5).

The crusts' mean of all median (mean median) particle diameters in the Mojave Desert reveal a coarser MDPSD compared to FDPSD, with values of 92 and 37 µm, respectively. In contrast, the mean median

https://doi.org/10.5194/egusphere-2024-434
Preprint. Discussion started: 27 February 2024

particle diameter is similar for aeolian ripples (226 and 213 µm, respectively) (Table S1). Analysing specific locations, the mean median particle diameter from the MDPSD of crusts varies, with the finest crust observed at Ivanpah Lake (35 µm) and the coarsest at Mesquite Lake (141 µm). Concerning FDPSD, the finest crust originates from Coyote Lake (8.4 µm), while the coarsest is from Soda Lake (52 µm) (Table S1). Similarly, for aeolian ripples, the mean median particle diameters for both MDPSD and FDPSD are finer at Mesquite Lake (167 and 67 µm, respectively) and coarser at Cronese lakes (264 and 234 µm, respectively) (Table S1). The high degree of particle aggregation observed in crusts, contrasting with the lower aggregation state in ripples, aligns with findings reported for dust-emitting sediments from Morocco by González-Romero et al. (2023).

The mean median particle diameters of sediments from dust-emitting regions in the Mojave Desert are similar to those from the Morocco crusts described by González-Romero et al. (2023). Specifically, the mean median MDPSD diameter for the Mojave Desert (92 ± 74 µm) closely resembles that of the Morocco Draâ Lower basin (113 ± 79 µm), albeit slightly finer, and is notably coarser than that of Iceland (55 ± 62 µm) (González-Romero et al., 2023, 2024). Furthermore, while the finest crust sampled in the Mojave Desert (Ivanpah with 35 µm) is slightly coarser than the finest from Morocco (L'Bour with 20 µm), the differences remain relatively small. For FDPSD, the coarsest crust average median particle diameter is from Iceland (56 ± 69 µm), followed by both Morocco and Mojave (37 ± 77 and 37 ± 48 µm, respectively). Additionally, average MDPSD median diameters of aeolian ripples from the Mojave Desert closely resemble those from Morocco (226 and 221 µm, respectively), while those from Iceland are slightly coarser (280 µm).

Close to the centre of the Soda Lake, where numerous crust samples were collected, before reaching massive crust cementation by evaporite minerals, the FDPSD median diameter reaches very fine sizes (8-15 µm) (Figure S1). In contrast, towards the edges of the basin (closer to the mountains surrounding this endorheic lake), the size markedly increases, ranging from 22 to 87µm (Figure S1). Similar patterns, yet with coarser sizes, are observed for the MDPSD. The fluctuation of the groundwater table in the centre of the basin leads to the massive precipitation of salts, resulting in the formation of compact crusts (Figure 4) that should effectively reduce dust emission. However, at the edges of this central part, where the precipitation of salts is less frequent, and reworking of the crusts by fluctuations in the groundwater occurs, salty and spongy crusts are formed (Figure 4). These spongy crusts, being less compact, are easily broken by saltating particles, potentially leading to frequent high-salt dust emissions. This particle size segregation, with finer particle diameters towards the centre of the lake, is derived from the transport of sediments from the surrounding mountains to the central part of the lake by runoff waters during rain episodes.

3.2. Mineralogy

The evaluation of the mineralogy of crusts and aeolian ripples is key identifying potential dust source markers in the emitted dust, and investigating size fractionation processes upon transport into the basins that may alter mineral contents compared to the background sediment mineralogy.

Dust emitting sediments from the Mojave Desert primarily consist of feldspars (41 ± 12 %, including albite/anorthite and microcline), quartz (22 ± 11 %) and clay minerals (18 ± 12 %, such as kaolinite, montmorillonite and illite). Additionally, minor contents of carbonate minerals (6.6 ± 6.6 %), amphibole (pargasite) 4.1 ± 1.5 %, and iron oxides (maghemite) 0.77 ± 0.54 % are observed (Figure 6,

https://doi.org/10.5194/egusphere-2024-434
Preprint. Discussion started: 27 February 2024

Tables 2 and S2). Moreover, at Soda, Mesquite and Cronese lakes, Na-salts such as halite, thenardite, trona, and burkeite are also present, with an average salt content 5.0 ± 11 %. Additionally, zeolites (0.77 ± 1.1% to 8.5%) including laumontite and analcime are detected at Soda, Cronese, and Coyote lakes (the southern ones), with the highest content observed at Coyote Lake. Gypsum is found at Mesquite Lake (15 ± 29 %) (Figure 6, Tables 2 and S2). Moreover, Mesquite Lake crusts exhibit high contents of dolomite and calcite (15 ± 11%) compared to other basins (3.6 ± 2.6% to 7.2%) (Table 2).

The overall mineral composition of the dust-emitting sediments originates primarily from the source rocks prevalent in the region. These include dominant granitic rocks of Mesozoic ages, as well as pre-Tertiary, Tertiary and Quaternary volcanics, and Pre-Cambrian and Mesozoic metamorphic rocks (Figure 1). In the northern, northeastern, and eastern areas of the Mesquite Lake, an important limestone and dolostone massif from the Palaeozoic serves as a significant source of sediments (Figure 1), contributing to the high content of calcite and dolomite in the sediments of this lake. The presence of zeolites may be attributed to the weathering of volcanic outcrops in the region or to precipitation in alkaline lakes.

In comparison to aeolian ripples, the average composition of Mojave Desert crusts shows slightly enrichment in clay minerals (24 ± 11 versus 7.8 ± 2.3 % in crust and ripples, respectively), carbonates (6.6 ± 6.6 versus 1.1 ± 2.2 %), Na-salts (7.3 ± 13 versus 1.1 ± 3.7 %), zeolites (1.2 ± 1.9 versus 0.12 ± 0.52 %) and maghemite (0.92 ± 0.59 versus 0.49 ± 0.28 %), while being depleted in quartz (16 ± 7.2 versus 32 ± 9.5 %), feldspars (37 ± 9.7 versus 48 ± 13 %) and gypsum (3.1 ± 14 versus 4.7 ± 20 %), with similar amphibole content (4.1 ± 1.5 versus 4.1 ± 1.6 %) (Figure 6, Tables 2 and S2).

The results demonstrate that crusts, in all cases, have a significant enrichment in clay minerals, Na-salts, zeolites, and maghemite, while being depleted in quartz and feldspars compared to ripples, except for the anthropogenically disturbed sediments in Mesquite Lake as discussed below (Table 2).

In the largest dust hotspot, Soda Lake, the concentration of Na-salts in crusts increases towards the inner part of the lake, ranging from 5-10 % at the edges to 45-50 % in the centre, where compact and fully salt-cemented crusts form. This phenomenon is illustrated in Figure 7, which presents a geological and mineralogical cross-section of Soda Lake. In addition to the water transport to this central part of the basin during the rain episodes, groundwater discharge from the Zzyzx mountains occurs. There, the groundwater table is close to the surface, and the high salinity of the aquifer causes the massive precipitation of Na-salts that consolidate the crusts (Figure 4). Cycles of precipitation and dissolution of the salts yield salty spongy crusts (Figure 4) at the edges of these massive crusts, with higher dust emission potential. The very high content of Na-salts content in Soda Lake is attributed to the continuous high Na-S-Cl groundwater supply in the vicinity of Zzyzx, defining Soda Lake as a wet playa lake according to Reynolds et al. (2009). On the other hand, Cronese, Coyote, and Ivanpah are categorized as dry lakes.

Mesquite Lake has been significantly disturbed by salt mining activities that were pumping groundwater to separate different salts for economic purposes. This generated very large amounts of gypsum at the surface that is now a major constituent of both dunes and crusts in the exploited area of the basin. Furthermore, piles of worked sediments and residues from the exploitation are an important source of sand and silt for dust emissions. The contents of Na-salts (7.5 and 14 % in and 30 % outside of the exploitation) and carbonate minerals (<0.1 and 6.9 % in and 12 and 18 % out of the exploitation) in crusts are higher at the edges, while that of gypsum is high at the centre of the

https://doi.org/10.5194/egusphere-2024-434
Preprint. Discussion started: 27 February 2024

exploitation (80 % in and 3.0 to 11 % outside of the exploitation). There, aeolian ripples exhibit a very high content of gypsum, originating from the precipitation of brines from salt exploitation and accumulation in waste piles, which supply gypsum grains for aeolian ripples throughout Mesquite. However, in the less anthropogenically disturbed borders, aeolian ripples also include quartz, feldspars, and clays.

Amphiboles in the Mojave Desert, sourced from metamorphic rocks of the area, are homogeneous and can serve as a marker for emitted desert dust in the region. Comparing mineralogy from Mojave Desert crusts to Moroccan surface samples (González-Romero et al., 2023), the former are largely enriched in feldspars, clay minerals, Na-salts, and gypsum, and depleted in quartz and carbonates, with trace proportions of amphibole, zeolites, and maghemite. Ripples in the Mojave Desert are depleted in quartz and carbonates, enriched in feldspars, clay minerals, Na-salts, and gypsum, with traces of amphibole, maghemite, and zeolites compared to Moroccan ripples. The mineralogy of the Mojave Desert is markedly different from that of Iceland, due to differences in bedrock geology, although both contain feldspars, zeolites, and maghemite (González-Romero et al., 2024).

Particle aggregation of the dust-emitting sediments from the Mojave Desert samples, similar to those described by González-Romero et al. (2023) for the Moroccan ones, is probably due to clays, Na-salts and precipitated carbonates presence. This aggregation inhibits aerodynamic entrainment and dust emission should be mostly controlled by saltation bombardment (Shao et al., 1993). The occurrence of crystalline Fe oxides is limited to maghemite, mainly a weathering product from magnetite, with no hematite, goethite or other Fe oxides were detected by XRD, in contrast to Moroccan crusts (González-Romero et al., 2023).

3.3. Mode of occurrence of Fe

The average content of FeT in the Mojave crusts is 3.0 ± 1.3 wt %, while for aeolian ripples is 1.9 ± 1.1 wt %. Among these crusts, 1.8 ± 0.92 % of the FeT occurs as FeA, 17 ± 7.2 % as FeD, 2.1 ± 1.2 as FeM and 79 ± 8.5 % as FeS (Tables 3 and S3). Aeolian ripples have very similar contents and modes of occurrence of Fe across the Mojave Desert.

Among the crusts, Ivanpah has the highest FeT content at 4.9 %, followed by Cronese and Coyote lakes (3.7 ± 1.2 % and 3.5 %, respectively), with Soda Lake showing a similar content (3.1 ± 1.2 %). Mesquite has the lowest FeT (1.6 ± 0.53 %), probably due to dilution of detrital Fe-bearing minerals with salts and gypsum. FeS is the dominant mode of occurrence in most lakes, ranging from 68 % (1 sample) at Ivanpah, to 74 ± 3.5 and 74 ± 13 % at Mesquite and Cronese, and to 83 ± 2.8 and 82 % at Soda and Coyote lakes. The FeD is higher at Ivanpah (29 %), Cronese and Mesquite (21 ± 11 and 20 ± 2.7 %), and lower at Soda and Coyote lakes (14 ± 2.5 and 14 %). The content of FeM is higher at Mesquite Lake (3.7 ± 1.2 %), followed by Cronese and Coyote lakes (2.3 ± 1.1 and 2.4 %), and Soda (1.5 ± 0.49 %) and Ivanpah Lakes (0.82 %). Finally, FeA is higher at Cronese Lake (2.4 ± 0.99 %), compared to Coyote, Mesquite, Soda and Ivanpah lakes (1.8, 1.8 ± 0.93, 1.5 ± 0.81 and 1.4 %) (Tables 3 and S3). Crusts are enriched in FeT, FeD and FeA compared to ripples, while ripples are enriched in FeM and FeS (Tables 3 and S3).

Thus, the bulk Fe content in crusts is driven by structural Fe from clays and amphiboles (as deduced from the high correlation shown in Figure 8a), followed by small proportions of hematite and goethite (not detected by XRD), which are clearly higher at the northern lakes Ivanpah and Mesquite lakes,

https://doi.org/10.5194/egusphere-2024-434
Preprint. Discussion started: 27 February 2024

probably due to the Precambrian and Cambrian metamorphic rocks that supply sediments. Furthermore, the easily exchangeable Fe is also driven by clay minerals (Figure 8b).

Compared to crusts in other arid regions analysed by González-Romero et al. (2023, 2024), Mojave Desert crusts have similar FeT content to Moroccan crusts but are much lower than the Iceland top sediments (3.0 ± 1.3, 3.6 ± 0.71 and 9.5 ± 0.39 %, for Mojave, Morocco, and Iceland respectively). The proportion of FeS in FeT is similar to the Icelandic sediments but higher than Moroccan samples (79 ± 8.5 and 79 ± 6.5 %, and 67 ± 2.4, respectively). The proportion of FeM is clearly lower than that of Iceland, but higher than that of Morocco (2.1 ± 1.2 and 16 ± 5.4 %, for Mojave and Iceland; Morocco proportion is negligible). The FeD proportion is intermediate between Morocco and Iceland (17 ± 7.2, 31 ± 2.3, 3.5 ± 1.5 %, respectively), while the FeA proportion is similar to both Morocco and Iceland crusts (1.8 ± 0.92, 1.3 ± 0.39 and 1.9 ± 0.55 %, respectively) (Figure 9).

4. Conclusions

The playa lakes sampled within the Mojave Desert serve as significant dust-emitting sources in the region. Descriptions provided by Urban et al. (2018) and satellite imagery (Figure 2) confirm the presence of desert dust emissions originated from these areas. The lithology, geological/tectonic evolution, and past and current climate conditions collectively contribute to the formation of these dust sources in the Mojave Desert.

Dust-emitting sediments in this region predominantly stem from substratum rocks, comprising mainly granitic and volcanic formations, along with metamorphic Pre-Cambrian, Cambrian, Paleozoic, and Mesozoic rocks. Endorheic basins, shaped by faulting during the Tertiary-Quaternary period, accumulated fine sediments through erosion, transportation, and deposition processes. Wetter conditions prevailing during the Pleistocene epoch led to the formation of deep lakes within the basins, which gradually desiccated as the climate evolved. These arid conditions rendered the playa lakes susceptible to dust emission under specific atmospheric conditions. Notably, a particle size segregation is observed, transitioning from coarser sediments in the proximal alluvial areas towards finer particle crusts within the central regions of the lakes. In the playa lakes, finer sediments accumulate towards the center of the lakes due to flood events inundating the central areas and ponding, which facilitates the deposition of coarser particles followed by top finer sediment sizes.

According to the conceptual model depicted in Figure 10, the finer dust particle size distributions (FDPSD) range from 8.4 to 99 µm inside Soda Lake and 46 to 111 µm outside Soda Lake (MDPSD), underscoring this sedimentation process. Comparisons with conceptual models proposed for other regions, such as those by González-Romero et al. (2023, 2024) for locations in Morocco and Iceland, reveal a similar transport fractionation phenomenon occurring in the Mojave Desert. These crusts, observed within Soda Lake, show enrichment in clay minerals, carbonate minerals, salts, and iron oxides, while experiencing depletion in coarser constituents such as feldspars and quartz.

In the Mojave Desert, two distinct types of playa lakes, characterized as wet and dry, are delineated based on the regime of the groundwater table and its interaction with the surface, as discussed by Reynolds et al. (2009) and Goudie (2018). Understanding the groundwater table regime is fundamental in this region due to its profound influence on the porosity of the crust and its consequential impact on mineralogy, including the precipitation and enrichment of salts (Figure 10).

This dynamic contrasts sharply with other conceptual models, where the relationship between crust formation and the groundwater table is either minimal or absent entirely. For instance, there is no or little relation between crusts and groundwater table in Morocco, and in Iceland, the water regime is largely influenced by floodings from glaciers (González-Romero et al., 2023, 2024). In wet playa lakes like Soda Lake, the presence of salty crusts, whether massive or spongy, is significantly pronounced. Conversely, in dry playa lakes such as Ivanpah, Coyote, and Cronese, the influence of salt crusts is notably less prominent (see Figure 10). Mesquite Lake serves as a poignant example of an anthropogenically disturbed playa lake, highlighting the importance of monitoring dust changes resulting from human actions in such environments.

At Soda Lake, a wet playa, a hard crust, measuring up to 0.5 meters in thickness (Figure 3), forms through the extensive precipitation of Na-salts, particularly near the Zzyzx area, where a relatively constant supply of salts is provided by the water table. Along the edges of this massive crusty area, the frequent oscillation of the water table results in the precipitation and dissolution of salts in lower quantities compared to the center, leading to the formation of weaker crusts characterized by high porosity. These porous crusts can contribute to an increased dust emission rate compared to the hard salt crusts found in the center. Dry lakes such as Ivanpah, Cronese, and Coyote do not exhibit the formation of spongy crusts due to the low concentrations of salts.

Particle aggregation facilitated by diagenetic salts and carbonate minerals is prevalent in the dust-emitting sediments of the Mojave Desert, akin to the equivalent sediments found in the Moroccan Sahara. The average grain size of the crusts from both regions is similar, with MDPSD values of 113 ± 79 µm for Morocco and 92 ± 74 µm for the Mojave Desert, and FDPSD values of 37 ± 77 µm and 37 ± 48 µm, respectively. These patterns contrast with the lower aggregation state and finer MDPSD observed in Icelandic dust (55 ± 62 µm) (Table 4).

In terms of mineralogy, crusts from the Mojave Desert are enriched in feldspars, clay minerals, Na-salts, and gypsum, whereas crusts from the Moroccan Sahara are enriched in quartz and carbonates (Table 4). The mineralogy of Icelandic top sediments differs due to their volcanic origin; however, both the Mojave Desert and Icelandic top sediments contain similar amounts of zeolites. Salt enrichment in the crusts is primarily attributed to interactions with the groundwater table (Figure 10).

The total iron content (FeT) remains consistent throughout the Mojave Desert, with slightly higher levels observed in the Ivanpah crust, albeit diluted by the high salt content in the wet playa lake crusts or the elevated gypsum content in the anthropogenically disturbed Mesquite Lake. While the total Fe content is comparable between the Mojave Desert and Moroccan Sahara crusts (3.0 and 3.6 wt %, respectively), it is substantially lower than in Icelandic top sediments (9.3 wt %). Exchangeable Fe proportions in FeT are similar among the three environments. The proportion of Fe from hematite and goethite in Mojave Desert crusts fall between those of Moroccan Sahara crusts and Icelandic top sediments (17, 31, and 0.5 wt %, respectively). The proportion of magnetite in Mojave Desert crusts is much lower compared to Icelandic top sediments (2.1 and 15 %, respectively). Finally, the proportion of structural Fe in the samples is similar across the three environments.

In conclusion, the dust-emitting sediments from the Mojave Desert exhibit distinct signatures in mineralogy and Fe mode of occurrence compared to those from the Moroccan Sahara, despite similar particle sizes. These differences can influence emitted dust properties, and associated impacts. Similarities in fully disturbed and minimally disturbed particle size distributions support comparable dust emission mechanisms, with saltation bombardment playing a prominent role. The mineralogy and Fe mode of occurrence of Mojave Desert dust significantly differ from Icelandic dust, potentially resulting in different radiative effects and oceanic and terrestrial fertilization.

Code availability. The Tetracorder code used in this paper is provided by Clark (2023, https://github.com/PSI-edu/spectroscopy-tetracorder).

Data availability. Data used in this paper are given in the main paper itself and in the Supplement. If needed, data are also available upon request by emailing the authors.

Author contribution. Sample permits were obtained by BLE, RG and AK. The samples were collected by CPG-P, AGR, AK, RG and XQ and analysed by AGR, MHC and NM. EMIT mineralogy maps we produced by RG, PB and RC. PG provided the FoO map. AGR analyzed the data and wrote of the original draft manuscript supervised by CPG-P and XQ. CPG-P and XQ re-edited the manuscript and all authors contributed to data discussion, reviewing and manuscript finalization.

Competing interests. At least one of the (co-)authors is a member of the editorial board of Atmospheric chemistry and Physics.

Acknowledgements

The field campaign and its associated research, including this work, was funded by the European Research Council under the Horizon 2020 research and innovation programme through the ERC Consolidator Grant FRAGMENT (grant agreement No. 773051) and the AXA Research Fund through the AXA Chair on Sand and Dust Storms at BSC. CGF was supported by a PhD fellowship from the Agència de Gestió d'Ajuts Universitaris i de Recerca (AGAUR) grant 2020_FI B 00678. KK was funded by the Deutsche Forschungsgemeinschaft (DFG, German Research Foundation) – 264907654; 416816480. MK has received funding through the Helmholtz Association's Initiative and Networking Fund (grant agreement no. VH-NG-1533). We acknowledge the EMIT project, which is supported by the NASA Earth Venture Instrument program, under the Earth Science Division of the Science Mission Directorate. We are grateful to Claire Blaske and Sahil Azad for assistance sampling in the Mojave National Preserve. Samples within the preserve were collected under permit MOJA-2022-SCI-0034. We thank Rose Pettiette at the BLM office in Needles, CA, for advice and allowing sampling on BLM land. We thank Jason Wallace and Anne Kelly from CSU Desert Studies Center at Zzyzx for their support during the campaign. BLE, RG, and AMK thank the Resnick Sustainability Institute at Caltech for partial support. Without all of them, the sampling campaign would not have been successfully feasible.

5. References

Arnalds, Ó., Olafsson, H. and Dagsson-Waldhauserova, P.: Quantification of iron-rich volcanogenic dust emissions and deposition over the ocean from Icelandic dust sources, Biogeosciences, 11, 6623-6632. https://doi.org/10.5194/bg-11-6623-2014, 2014.

Atkinson, J. D., Murray, B. J., Woodhouse, M. T., Whale, T. F., Baustian, K. J., Carslaw, K. S., ... & Malkin, T. L.: The importance of feldspar for ice nucleation by mineral dust in mixed-phase clouds. Nature, 498(7454), 355-358, 2013.

Baldo, C., Formenti, P., Nowak, S., Chevaillier, S., Cazaunau, M., Pangui, E., Di Baggio, C., Doussin, J.F., Ignatyev, K., Dagsson-Waldhauserova, P., Arnalds, O., MacKenzie, A.R., Shi, Z.: Distinct chemical and mineralogical composition of Icelandic dust compared to Northern African and Asian dust. Atmospheric Chemistry and Physics, 20, 13521-13539, 2020.
Bauer, S. E., & Koch, D.: Impact of heterogeneous sulfate formation at mineral dust surfaces on aerosol loads and radiative forcing in the Goddard Institute for Space Studies general circulation model. Journal of Geophysical Research: Atmospheres, 110(D17), 2005.
Beaudoing, H., Rodell, M., & NASA/GSFC/HSL: GLDAS Noah Land Surface Model L4 monthly 0.25 x 0.25 degree, Version 2.1 [dataset]. NASA Goddard Earth Sciences Data and Information Services Center. 2020. https://doi.org/10.5067/SXAVCZFAQLNO.
Chatziparaschos, M., Daskalakis, N., Myriokefalitakis, S., Kalivitis, N., Nenes, A., Gonçalves Ageitos, M., Costa-Surós, M., Pérez García-Pando, C., Zanoli, M., Vrekoussis, M. & Kanakidou, M.: Role of K-feldspar and quartz in global ice nucleation by mineral dust in mixed-phase clouds. Atmospheric Chemistry and Physics, 23(3), 1785-1801, 2023.
Cheary, R.W., Coelho, A.: A fundamental parameters approach to X-ray line profile fitting. Journal of Applied Crystallography 25, 109–121, 1992.
Clark, R. N., Swayze, G. A., Livo, K. E., Brodrick, P., Noe Dobrea, E., Vijayarangan, S., Green, R. O., Wettergreen, D., Garza, A. C., Hendrix, A., García-Pando, C. P., Pearson, N., Lane, M., González-Romero, A., Querol, X. & the EMIT and TREX teams. Imaging spectroscopy: Earth and planetary remote sensing with the PSI Tetracorder and expert systems: from Rovers to EMIT and Beyond, Planetary Science J., in review, 2023.
Crumeyrolle, S., Gomes, L., Tulet, P., Matsuki, A., Schwarzenboeck, A., and Crahan, K.: Increase of the aerosol hygroscopicity by cloud processing in a mesoscale convective system: a case study from the AMMA campaign, Atmos. Chem. Phys., 8, 6907–6924, https://doi.org/10.5194/acp-8-6907-2008, 2008.
De la Torre, A.G., Bruque, S., Aranda, M.A.G.: Rietveld quantitative amorphous content analysis. Journal of Applied Crystallography, 34:196-202, 2001.
De Longueville, F., Hountondji Y.C., Henry S., Ozer P.: What do we know about effects of desert dust on air quality and human health in West Africa compared to other regions?. Sci. Total Environ., 409, 1–8, 2010.
Dibblee T.W.: Areal geology of the western mojave desert California. Geological Survey Professional paper, 522, https://doi.org/10.3133/pp522, 1967.
Di Biagio, C., Formenti, P., Balkanski, Y., Caponi, L., Cazaunau, M., Pangui, E., Journet, E., Nowak, S., Andreae, M.O., Kandler, K., Saeed, T., Piketh, S., Seibert, D., Williams, E., Doussin, J.F.: Complex refractive indices and single-scattering albedo of global dust aerosols in the shortwave spectrum and relationship to size and iron content. Atmos. Chem. Phys., 19, 15503-15531. https://doi.org/10.5194/acp-19-15503-2019, 2019.
Eghbal, M.K., Southard, R.J.: Mineralogy of Aridisols on Dissected Alluvial Fans, Western Mojave Desert, California. Soil Science Society of America Journal, 57, pp. 538-544, 1993.
Engelbrecht, J.P., Moosmüller, H., Pincock, S., Jayanty, R.K.M., Lersch, T., Casuccio, G.: Technical note: Mineralogical, chemical, morphological, and optical interrelationships of mineral dust re-suspensions. Atmos. Chem. Phys., 16, 10809-10830. https://doi.org/10.5194/acp-16-10809-2016, 2016.
Formenti, P., Caquineau, S., Chevaillier, S., Klaver, A., Desboeufs, K., Rajot, J.L., Belin, S., Briois, V.: Dominance of goethite over hematite in iron oxides of mineral dust from Western Africa:

Quantitative partitioning by X-ray absorption spectroscopy. J. Geophys. Res. Atmos., 119, 12740-12754, https://doi.org/10.1002/2014jd021668, 2014.

Frank, T.D., Di Girolamo, L., Geegan, S.: The spatial and temporal variability of aerosol optical depths in the Mojave desert of southern California. Remote Sensing of Environment, 107, 1-2, 54-64, https://doi.org/10.1016/j.rse.2006.06.024, 2007.

Ginoux, P., Prospero, J.M., Gill, T.E., Hsu, N.C., Zhao, M.: Global-scale attribution of anthropogenic and natural dust sources and their emission rates based on MODIS Deep Blue aerosol products. Rev. Geophys., 50, RG3005, doi:10.1029/2012RG000388, 2012.

Goldstein, H.L., Breit, G.N., & Reynolds, R.L.: Controls on the chemical composition of saline surface crusts and emitted dust from a wet playa in the Mojave Desert (USA). Journal of Arid Environments, 140, 50-66, 2017.

González-Romero, A., González-Florez, C., Panta, A., Yus-Díez, J., Reche, C., Córdoba, P., Moreno, N., Alastuey, A., Kandler, K., Klose, M., Baldo, C., Clark, R.N., Shi, Z.B., Querol, X., Pérez García-Pando, C.: Variability in grain size, mineralogy, and mode of occurence of Fe in surface sediments of preferential dust-source inland drainage basins: The case of the Lower Drâa Valley, S Morocco. Atmos. Chem. Phys., 23, 15815–15834, https://doi.org/10.5194/acp-23-15815-2023, 2023.

González-Romero, A., González-Florez, C., Panta, A., Yus-Díez, J., Córdoba, P., Alastuey, A., Moreno, N., Kandler, K., Klose, M., Clark, R.N., Ehlmann, B.L., Greenberger, R., Keebler, A.M., Brodick, P., Green, R., Querol, X., Pérez García-Pando, C.: Probing Iceland's Dust-Emitting Sediments: Particle Size Distribution, Mineralogy, Cohesion, Fe Mode of Occurrence, and Reflectance Spectra Signatures. Atmospheric Chemistry and Physics. EGUSPHERE [Preprint], 2024.

Goudie, A.: Dust storms and ephemeral lakes. Desert, 23(1), 153-164, 2018.

Goudie, A.S. & Middleton, N.J.: Desert dust in the global system. Springer, Heidelberg. ISBN 978-786 3-540-32355-6, 288 pp, 2006.

Green R.O., Mahowald N., Ung C., Thompson D.R., Bator L., Bennet M., Zan J.: The earth surface mineral dust source investigation: an earth science imaging spectroscopy mission. In: IEEE Aerospace Conference Proceedings. IEEE Computer Society. https://doi.org/10.1109/AERO47225.2020.9172731. 2020.

Harrison, A. D., Lever, K., Sanchez-Marroquin, A., Holden, M. A., Whale, T. F., Tarn, M. D., ... & Murray, B. J.: The ice-nucleating ability of quartz immersed in water and its atmospheric importance compared to K-feldspar. Atmospheric Chemistry and Physics, 19(17), 11343-11361, 2019.

Honke, J.S., Pigati, J.S., Wilson, J., Bright, J., Goldstein, H.L., Skipp, G.L., Reheis, M.C., Havens, J.C.: Late Quaternary paleohydrology of desert wetlands and pluvial lakes in the Soda Lake basin, central Mojave Desert, California (USA). Quat. Sci. Rev., 216, pp. 89-106, 10.1016/j.quascirev.2019.05.021, 2019.

Ibáñez, J., Font, O., Moreno, N., Elvira, J.J., Alvarez, S., Querol, X.: Quantitative Rietveld analysis of the crystalline and amorphous phases in coal fly ashes. Fuel, 105: 314-317, 2013.

Jennings, C.W., Burnett, J.L., and Troxel, B.W.: Geologic map of California: Trona sheet. California Division of Mines and Geology, Geologic Atlas of California, GAM-23, 1:250.000, 1962.

Jickells, T. D., An, Z. S., Andersen, K. K., Baker, A. R., Bergametti, G., Brooks, N., ... & Torres, R.: Global iron connections between desert dust, ocean biogeochemistry, and climate. science, 308(5718), 67-71, 2005.

Karanasiou, A., Moreno, N., Moreno, T., Viana, M., de Leeuw, F., Querol, X.: Health effects from Sahara dust episodes in Europe: Literature review and research gaps. Environ. Int. 47, 107–14, 2012.

https://doi.org/10.5194/egusphere-2024-434
Preprint. Discussion started: 27 February 2024

Kok, J.F., Adebiyi, A.A., Albani, S., Balkanski, Y., Checa-Garcia, R., Chin, M., Colarco, P.R., Hamilton, D.S., Huang, Y., Ito, A., Klose, M., Li, L., Mahowald, N.M., Miller, R.L., Obiso, V., Pérez García-Pando, C., Rocha-Lima, A., Wan, J.S.: Contribution of the world's main dust source regions to the global cycle of desert dust, Atmos. Chem. Phys., 21, 8169–8193, https://doi.org/10.5194/acp-21-8169-2021, 2021.

Laurent, B., Marticorena, B., Bergametti, G., Léon, J.F., Mahowald, N.M.: Modeling Mineral Dust Emissions from the Sahara Desert Using New Surface Properties and Soil Database J. Geophys. Res., 113, D14218, 2008.

Machiels, L., Mertens, G., Elsen, J.: Rietveld Refinement strategy for Quantitative Phase analysis of Partially Amorphous zeolitized tuffaceous. GEOLOGICA BELGICA 13,3, 183-196, 2010.

Madsen, I.C., Scarlett, N.V.Y., Cranswick, L.M.D., Lwin, T.: Outcomes of the international union of crystallography commission on powder diffraction round robin on quantitative phase analysis: Samples 1a to 1h. J. Appl. Crystallogr., 34, pp. 409-426, 2001.

Mahowald, N.M., Baker, A.R., Bergametti, G., Brooks, N., Duce, R.A., Jickells, T.D., Kubilay, N., Prospero, J.M., Tegen, I.: Atmospheric global dust cycle and iron inputs to the ocean, Global Biogeochem. Cy., 19(4), GB4025, doi:10.1029/2004GB002402, 2005.

Matsui, H., Yamane, M., Tonami, T., Nagami, T., Watanabe, K., Kishi, R., Kitagawa, Y., Nakano, M.: Theoretical study on gigantic effect of external static electric field application on nonlinear optical properties of 1,2,3,5-dithiadiazolyl π-radical dimer. Mater. Chem. Front., 2, 785– 790, DOI: 10.1039/C7QM00549K, 2018.

Miller, D.M., Menges, C.M., and Lidke, D.J.: Generalized surficial geologic map of the Fort Irwin area, San Bernardino County, California, U.S. Geological Survey, Open-File Report OF-2013-1024-B, 1:100.000, 2014.

Miller, D.M., Dudash, S.L., & McGeehin, J.P.: Paleoclimate record for Lake Coyote, California, and the Last Glacial Maximum and deglacial paleohydrology (25 to 14 cal ka) of the Mojave River. S.W. Starratt, M.R. Rosen (Eds.), From Saline to Freshwater: The Diversity of Western Lakes in Space and Time: Geologic Society of America Special Paper 536, pp. 1-20, 2018.

Pérez, C., Nickovic, S., Pejanovic, G., Baldasano, J. M., & Özsoy, E.: Interactive dust-radiation modeling: A step to improve weather forecasts. Journal of Geophysical Research: Atmospheres, 111(D16), 2006.

Pérez García-Pando, C., Stanton, M.C., Diggle, P.J., Trzaska, S., Miller, R.L., Perlwitz, J.P., Baldasano, J.M., Cuevas, E., Ceccato, P., Yaka, P., Thomson, M.C.: Soil dust aerosols and wind as predictors of seasonal meningitis incidence in Niger. Environ. Health Perspect. 122, 7679-686, 2014.

Perlwitz, J.P., Pérez García-Pando, C., and Miller, R.L.: Predicting the mineral composition of dust aerosols – Part 1: Representing key processes. Atmos. Chem. Phys., 15, 11593–11627, https://doi.org/10.5194/acp-15-11593-2015, 2015.

Potter, C. and Coppernoll-Houston, D.: Controls on land surface temperature in deserts of southern california derived from MODIS satellite time series analysis, 2000 to 2018. Climate, 7, 32, https://doi.org/10.3390/cli7020032, 2019.

Querol, X.: The Occurrence and Distribution of Trace Elements in the Teruel Mining District Coals and their Behaviour during Coal Combustion. European Coal and Steel Community Project 7220/ED/014, 1993.

Querol, X., Whateley, M.K.G., Fernandez-Turiel, J.L., Tuncali, E.: Geological controls on the mineralogy and geochemistry of the Beypazari lignite, Central Anatolia, Turkey. Int. J. Coal. Geol., 33:255–271, 1997.

Raupach, M.R., Gillette, D.A., Leys, J.F.: The effect of roughness elements on wind erosion threshold. J. Geophys. Res., 98, 3023-3029, 1993.

Reheis, M.C., Bright, J., Lund, S.P., Miller, D.M., Skipp, G., Fleck, R.J.: A half-million-year record of paleoclimate from the Lake Manix core, Mojave Desert, California. Palaeogeogr., Palaeoclim. Palaeoecol., 365–366, pp. 11-37, 2012.

Reynolds, R.L., Bogle, R., Vogel, J., Goldstein, H., Yount, J.: Dust emission at Franklin Lake Playa, Mojave Desert (USA): Response to meteorological and hydrologic changes 2005–2008, in: Oren, A., Naftz, D. L., Wurtsbaugh, W. A. (Eds.), Saline lakes around the world: unique systems with unique values, Natural Resources and Environmental Issues 15, 105–116, https://digitalcommons.usu.edu/nrei/vol15/iss1/18 (last access: 7 November 2023), 2009.

Rietveld, H.M.: A profile refinement method for nuclear and magnetic structures. Journal of Applied Crystallography 2, 65–71, 1969.

Scarlett, N. & Madsen, I.: Quantification of phases with partial or no known crystal structures. Powder Diffraction, 21(4), 278-284, 2006.

Shao, Y., Raupach, M.R., & Findlater, P.A.: Effect of saltation bombardment on the entrainment of dust by wind. Journal of Geophysical Research: Atmospheres, 98(D7), 12719-12726, 1993.

Shi, Z.B., Krom, M.D., Bonneville, S.: Formation of Iron Nanoparticles and Increase in Iron Reactivity in Mineral Dust during Simulated Cloud Processing. Environ. Sci. Technol. 43, 6592-6596, 2009.

Sperazza, M., Moore, J.N., Hendrix, M.: High-Resolution particle size analysis of naturally occurring very fine-grained sediment through laser diffractometry. J. Sediment. Res., 74 (5), 736-743, 2004.

Sullivan, R.C., Guazzotti, S.A., Sodeman, D.A., Tang, Y., Carmichael, G.R., & Prather, K.A.: Mineral dust is a sink for chlorine in the marine boundary layer. Atmospheric Environment, 41(34), 7166–7179, 2007.

Thorez, J.: Practical Identification of Clay Minerals: A Handbook for Teachers and Students in Clay Mineralogy. Institute of mineralogy, Liège State University, Belgium, Lelotte Eds, B 4820 DISON (Belgique),90pg, 1976.

Tong, D.Q., Dan, M., Wang, T., Lee, P.: Long-term dust climatology in the western United States reconstructed from routine aerosol ground monitoring, Atmos. Chem. Phys., 12, 5189–5205, https://doi.org/10.5194/acp-12-5189-2012, 2012.

TOPAS: TOPAS and TOPAS-Academic: an optimization program integrating computer algebra and crystallographic objects written in C++. J. Appl. Cryst. (2018). 51, 210-218, 2018.

Urban, F.E., Reynolds, R.L., Fulton, R.: The dynamic interaction of climate, vegetation, and dust emission, Mojave Desert, USA. A. Fernandez-Bernal, M.A. De La Rosa (Eds.), Arid Environments and Wind Erosion, NOVA Science Publishers, Inc., pp. 243-267, 2009.

Urban, F.E., Goldstein, H.L., Fulton, R., Reynolds, R.L.: Unseen dust emission and global dust abundance: documenting dust emission from the Mojave Desert (USA) by daily remote camera imagery and wind-erosion measurements. J. Geophys. Res. Atmos., 123 (16), pp. 8735-8753, 2018.

USGS, U. S. Geological Survey Open-File Report 01-041. A Laboratory Manual for X-Ray Powder Diffraction https://pubs.usgs.gov/of/2001/of01-041/htmldocs/methods/oamount.htm. Last access: 17th January of 2024.

Weaver, C., Ginoux, P., Hsu, N., Chou, M.-D., Joiner, J.: Radiative forcing of Saharan dust: GOCART model simulations compared with ERBE data. J. Atmos. Sci., 59, 736-747, 2002.

Whitney, J.W., Breit, G.N., Buckingham, S.E., Reynolds, R.L., Bogle, R.C., Luo, L., Goldstein, H.L., Vogel, J.M.: Aeolian responses to climate variability during the past century on Mesquite Lake Playa, Mojave Desert. Geomorphology, 230, 13-25, 2015.

Young, R.A.: The Rietveld method. International Union of Crystallography. Oxford University Press, UK, 1993.

Zubko, N., Munoz, O., Zubko, E., Gritsevich, M., Escobar-Cerezo, J., Berg, M. J. and Peltoniemi, J.: Light scattering from volcanic-sand particles in deposited and aerosol form. Atmospheric Environment, 215, 116813. https://doi.org/10.1016/j.atmosenv.2019.06.051, 2019.

Figure captions:

Figure 1: Study area map including the playa lakes studied together with a geologic map, simplified from Jennings et al. (1962) and Miller et al. (2014). The star represents the Zzyzx complex. Basemap: Imagery data from © Google Earth Pro v: 7.3.6.9345.

Figure 2: Map of Frequency of Occurrence (FoO) of dust optical depth > 0.1 over the study region derived from MODIS C6.1 Aqua (1:30PM equatorial passing time) Level 2 Deep Blue aerosol products at 0.1 degree resolution. A dust occurrence is counted when AOD > 0.1, Angstrom Exponent < 0.3 and AOD at 412 nm > AOD at 470 nm. Blue iso-contours represent 2, 5 and 10 % of daily occurrences per year averaged over 20 years (2003-2022). Basemap: Imagery data from © Google Earth Pro v: 7.3.6.9345.

Figure 3: EMIT scenes emit20231015T215209_color-visRGB and emit20230728T214142_color-visRGB at 60 m per pixel showing the diversity of Fe^{2+}, Fe^{3+} and Fe^{2+} and Fe^{3+} bearing minerals and the carbonates, salt and phyllosilicates minerals.

Figure 4: Examples of samples collected in the Mojave Desert including crusts (a), aeolian ripples (b), massive compact crust (c) and a salty spongy crust (d).

Figure 5: Fully dispersed particle size distribution (FDPSD) and minimally dispersed particle size distribution (MDPSD) for crusts and aeolian ripples from the Mojave Desert (median PSD from all the samples), Soda, Mesquite, Cronese, Ivanpah and Coyote Lakes. In shaded blue and brown the standard deviation of each PSD (nº of samples used in Table 1), except for Ivanpah and Coyote Lakes (only 1 sample each).

Figure 6: Box-plot showing averaged mineral contents for all samples, crusts and aeolian ripples (wt %).

Figure 7: Geological cross section and mineralogy of the crusts of the Soda Lake. Top panel represent major mineralogy composition. Mid panel represents the position of the samples, the Zzyzx complex, and the path of the cross section. Bottom schematic cross section simplifying the position in the basin. Basemap: Imagery data from © Google Earth Pro v: 7.3.6.9345.

Figure 8: Cross-correlation plots of the clay contents and amphibole with the FeT (a) and clay minerals and FeA (b), all in wt % in crusts.

Figure 9: Fe mode of occurrence comparison between the crusts (C) playa lakes analysed in this study, the average of the crusts and ripples (R) at Mojave Desert, Morocco and Iceland Top surface (TS). FeA is referred to the exchangeable Fe and nano Fe oxides, FeD is the Fe content in hematite and goethite, FeM is the Fe content in magnetite and FeS is the Fe content in Fe bearing minerals.

Figure 10: Conceptual model of wet and dry playa lakes differences due to groundwater differences and how this can affect the mineralogy of the surface in the playa lakes. Also illustrated is the expected dust emission rate, major mineralogy and Fe mode of occurrence differences expected in the emitted dust.

https://doi.org/10.5194/egusphere-2024-434
Preprint. Discussion started: 27 February 2024

Figure 1.

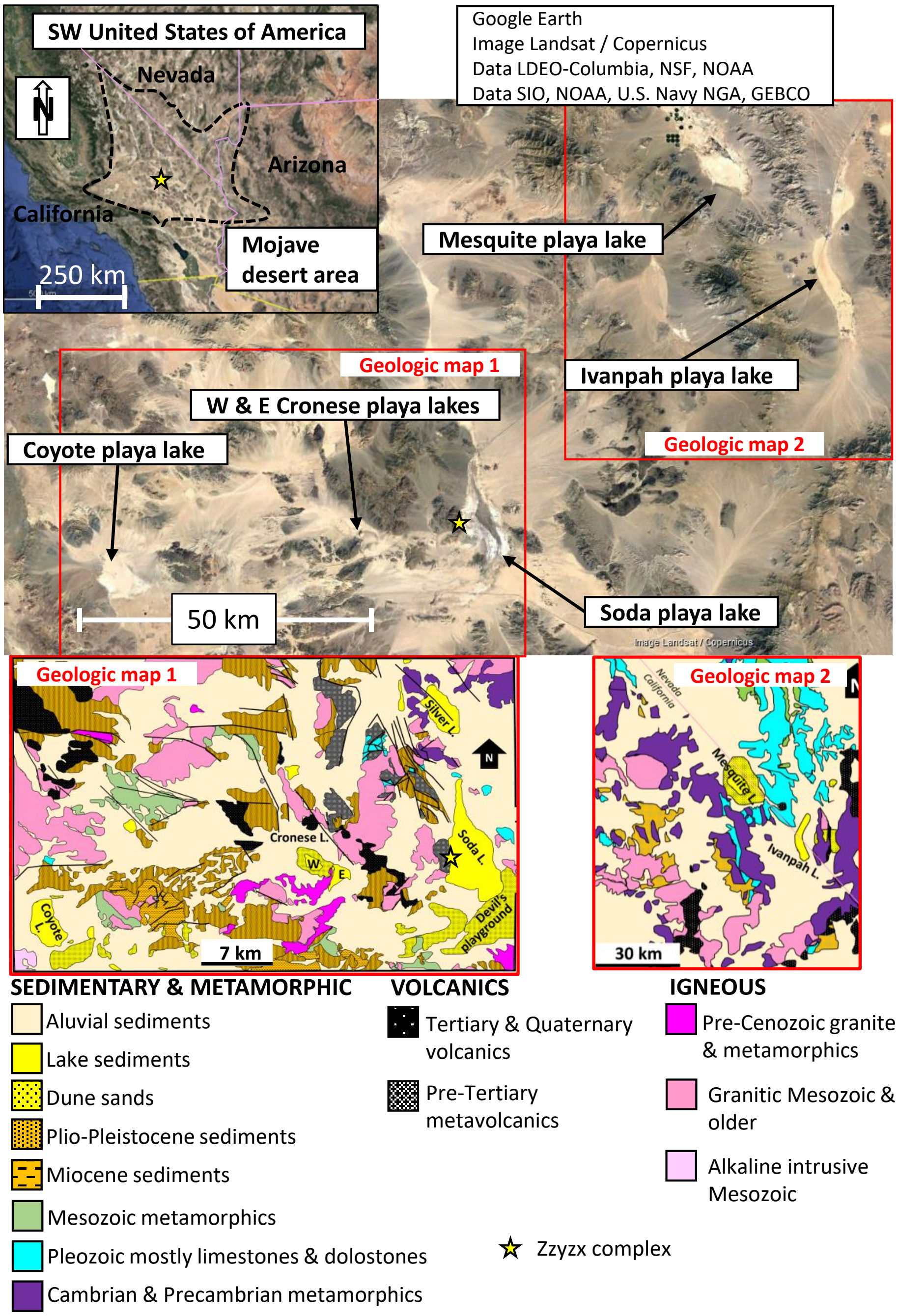

https://doi.org/10.5194/egusphere-2024-434
Preprint. Discussion started: 27 February 2024

Figure 2.

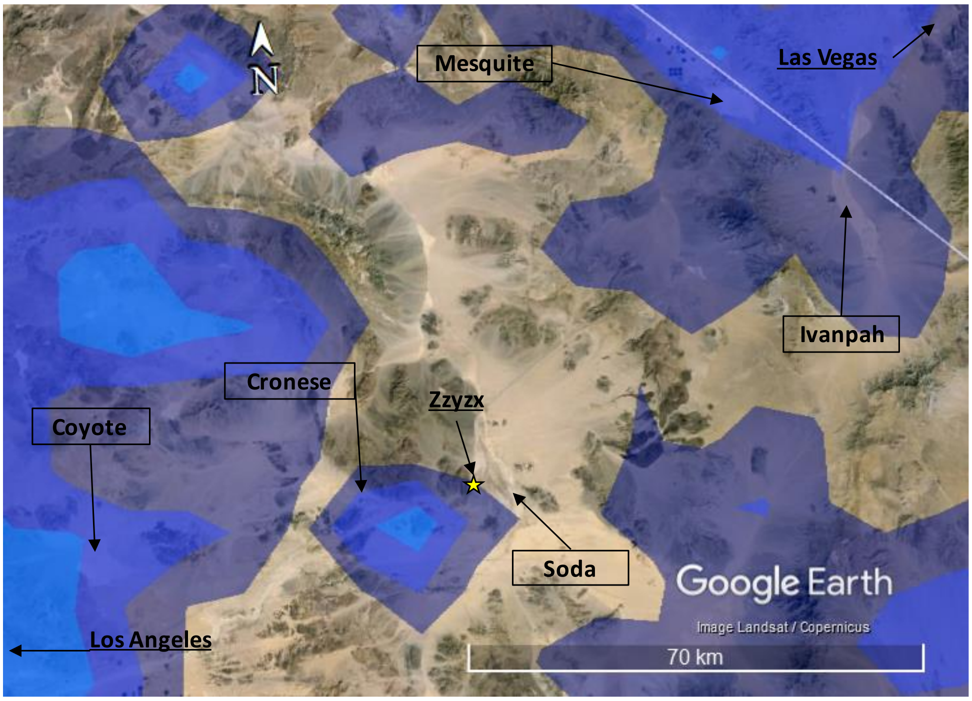

https://doi.org/10.5194/egusphere-2024-434
Preprint. Discussion started: 27 February 2024

762 Figure 3.

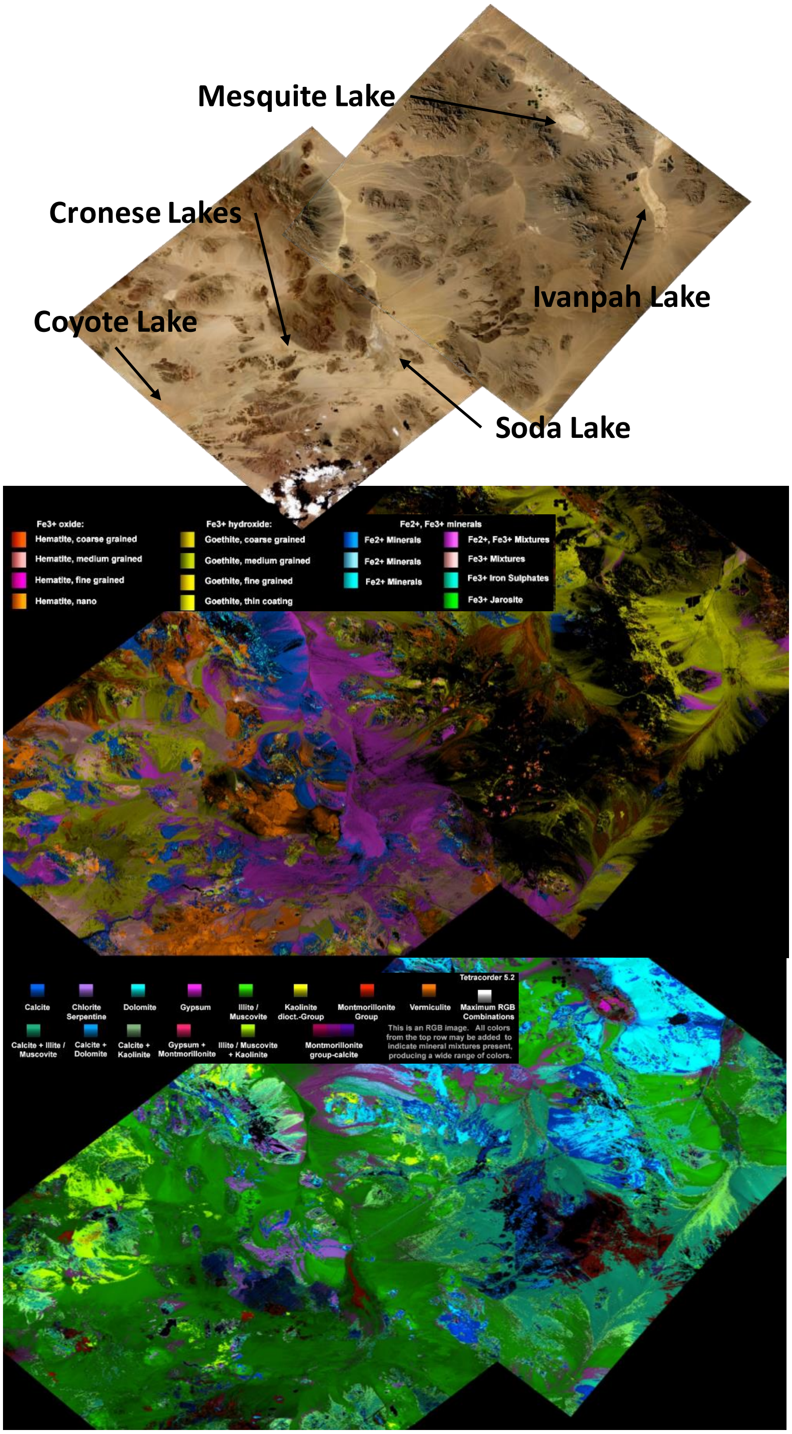

763

https://doi.org/10.5194/egusphere-2024-434
Preprint. Discussion started: 27 February 2024

Figure 4.

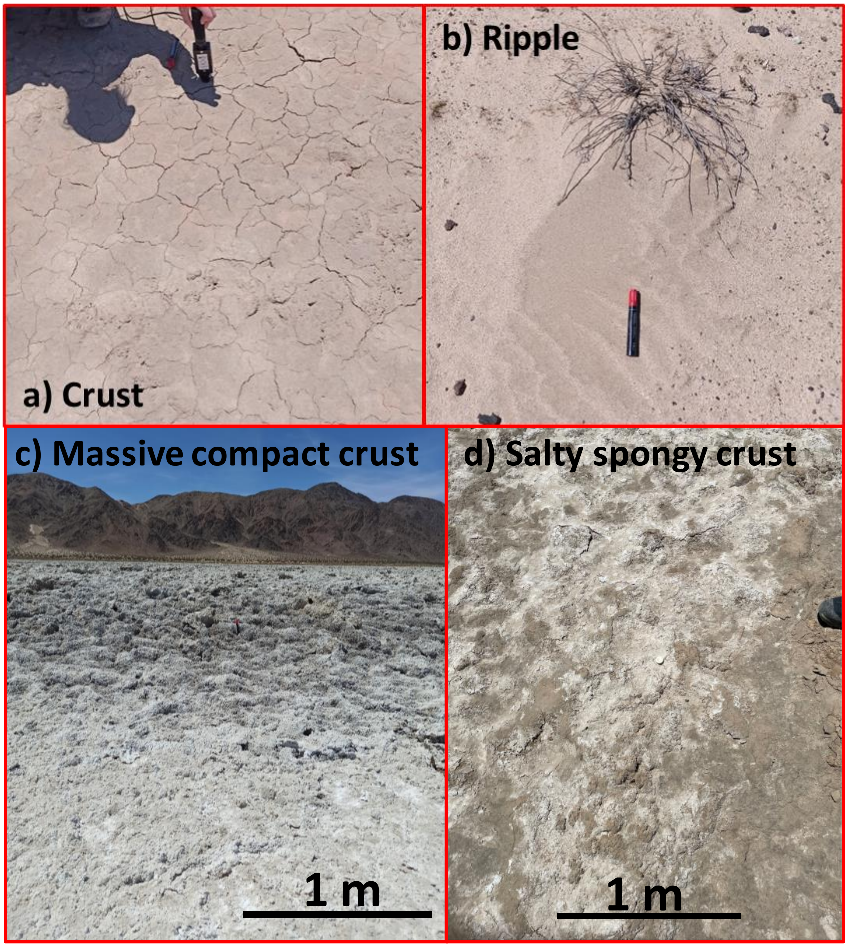

https://doi.org/10.5194/egusphere-2024-434
Preprint. Discussion started: 27 February 2024

Figure 5.

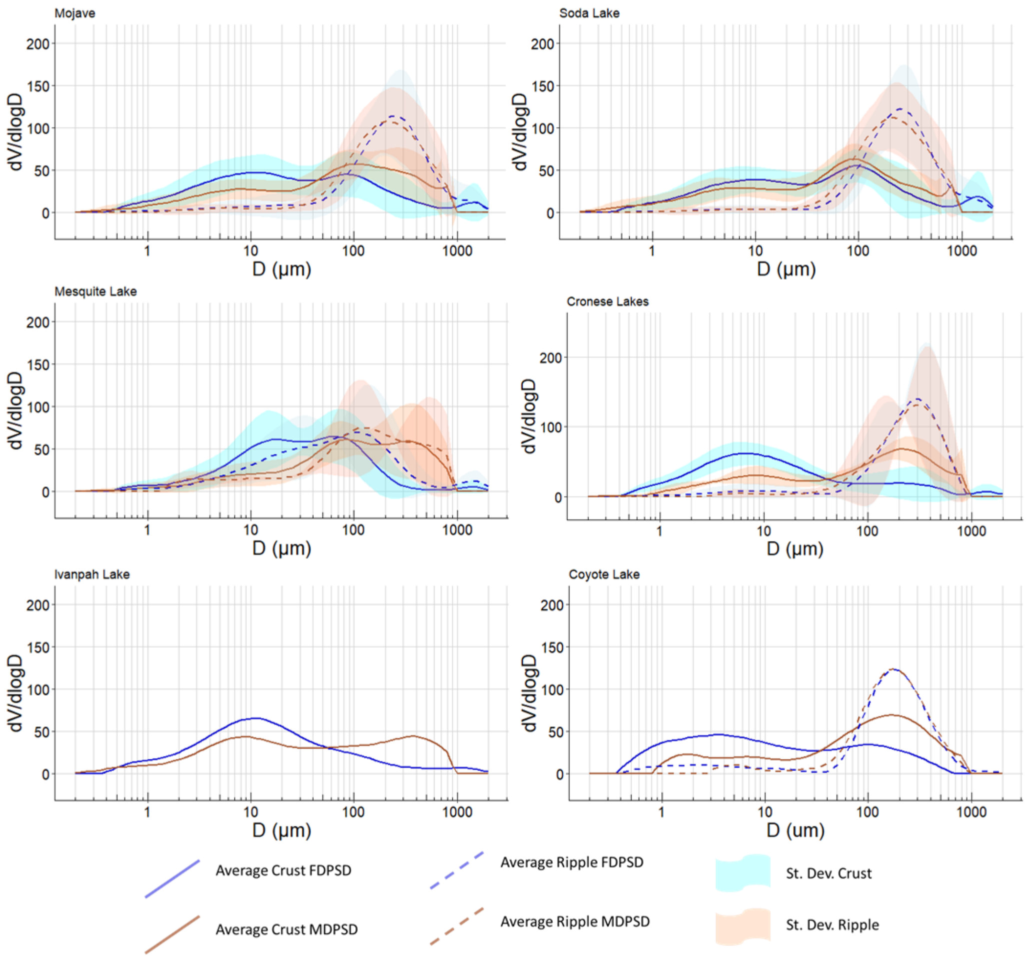

https://doi.org/10.5194/egusphere-2024-434
Preprint. Discussion started: 27 February 2024

Figure 6.

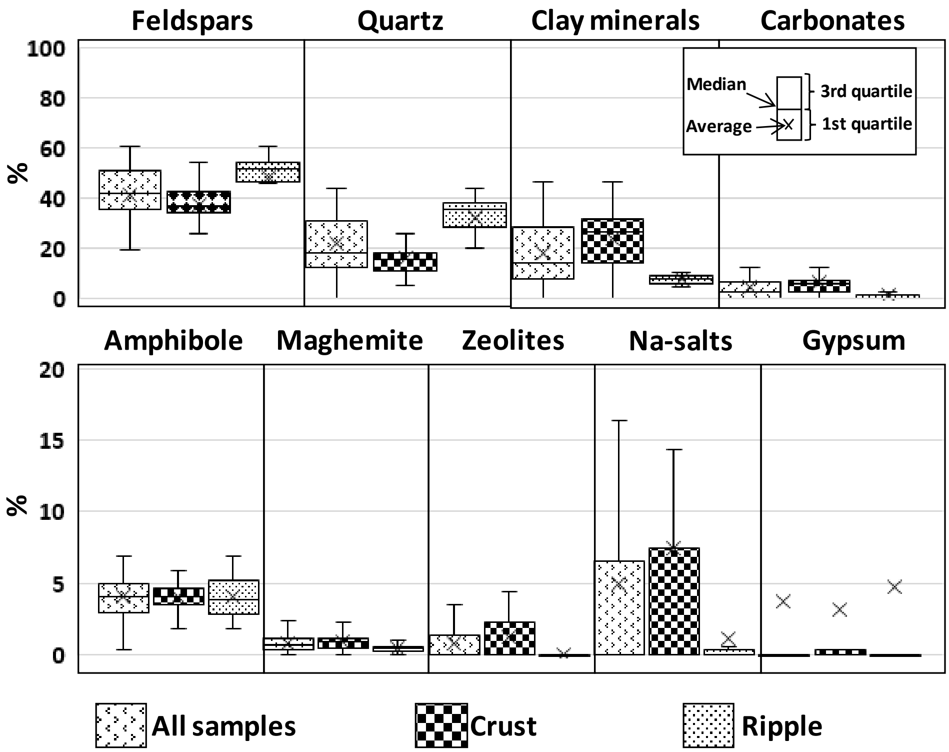

https://doi.org/10.5194/egusphere-2024-434
Preprint. Discussion started: 27 February 2024

Figure 7.

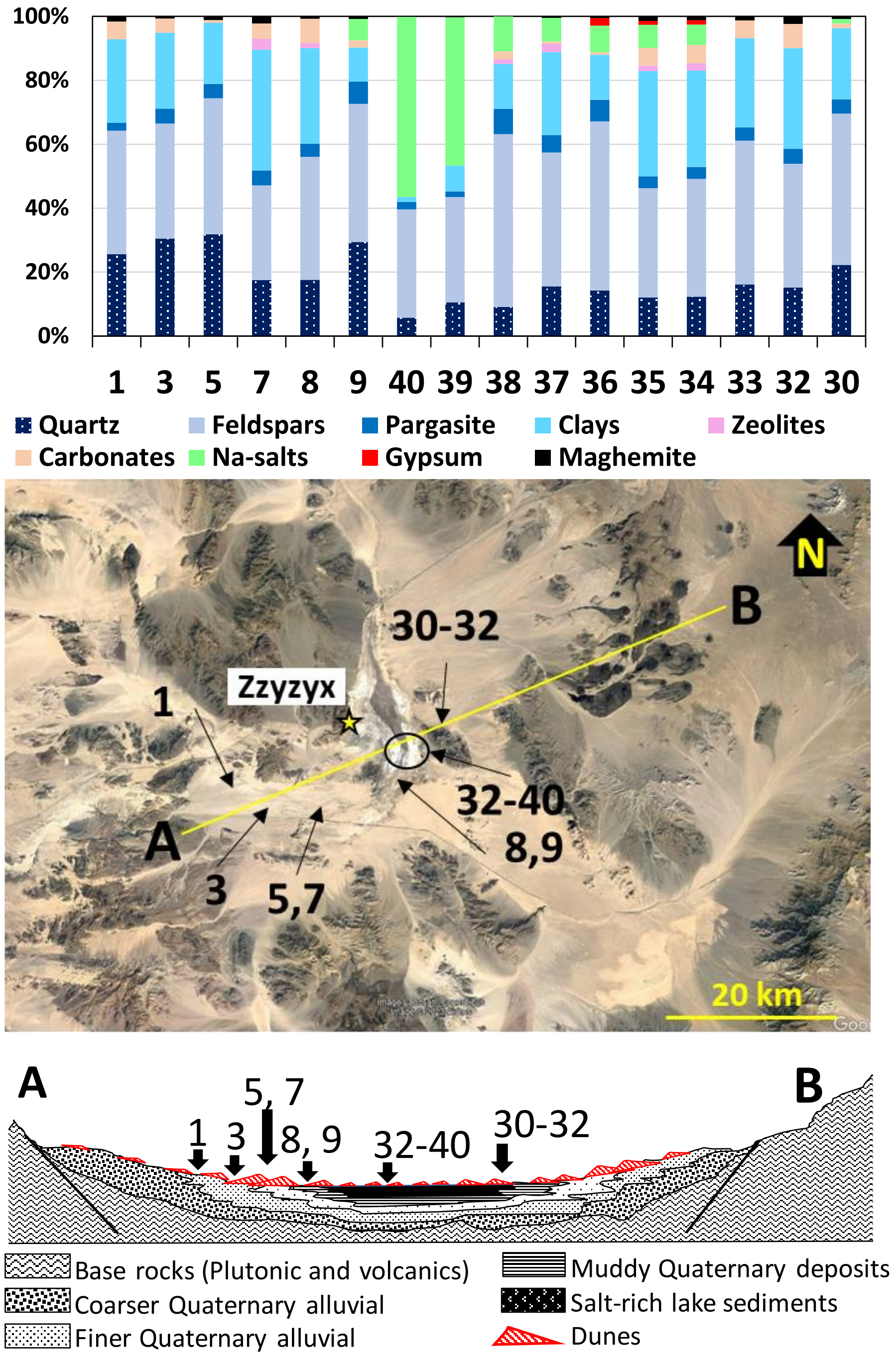

https://doi.org/10.5194/egusphere-2024-434
Preprint. Discussion started: 27 February 2024

Figure 8.

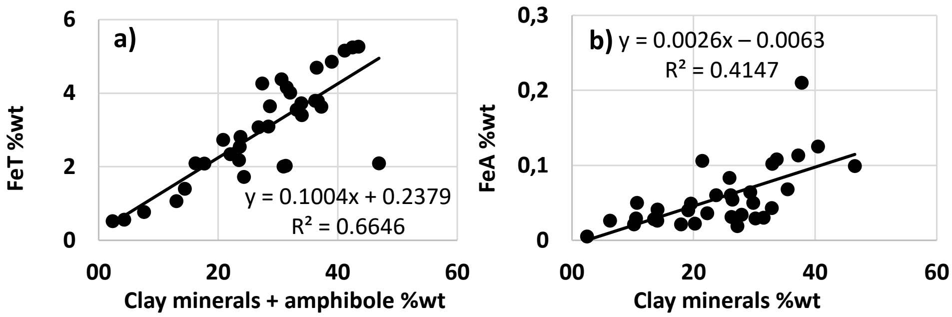

https://doi.org/10.5194/egusphere-2024-434
Preprint. Discussion started: 27 February 2024

Figure 9.

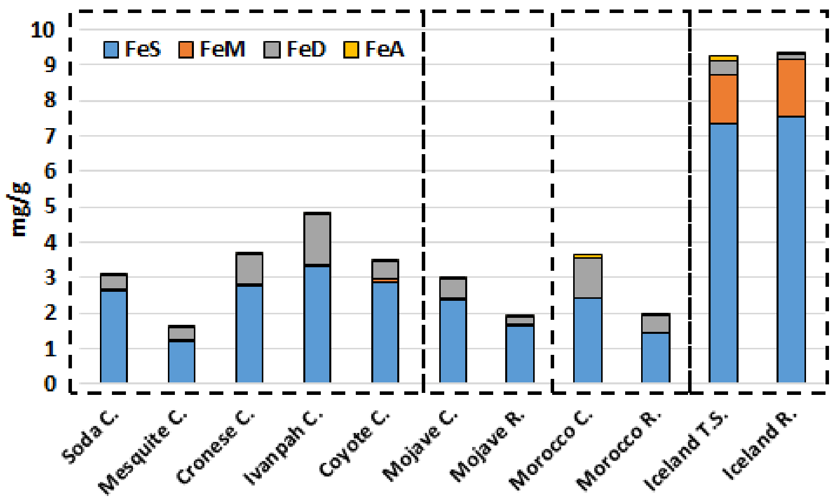

https://doi.org/10.5194/egusphere-2024-434
Preprint. Discussion started: 27 February 2024

Figure 10.

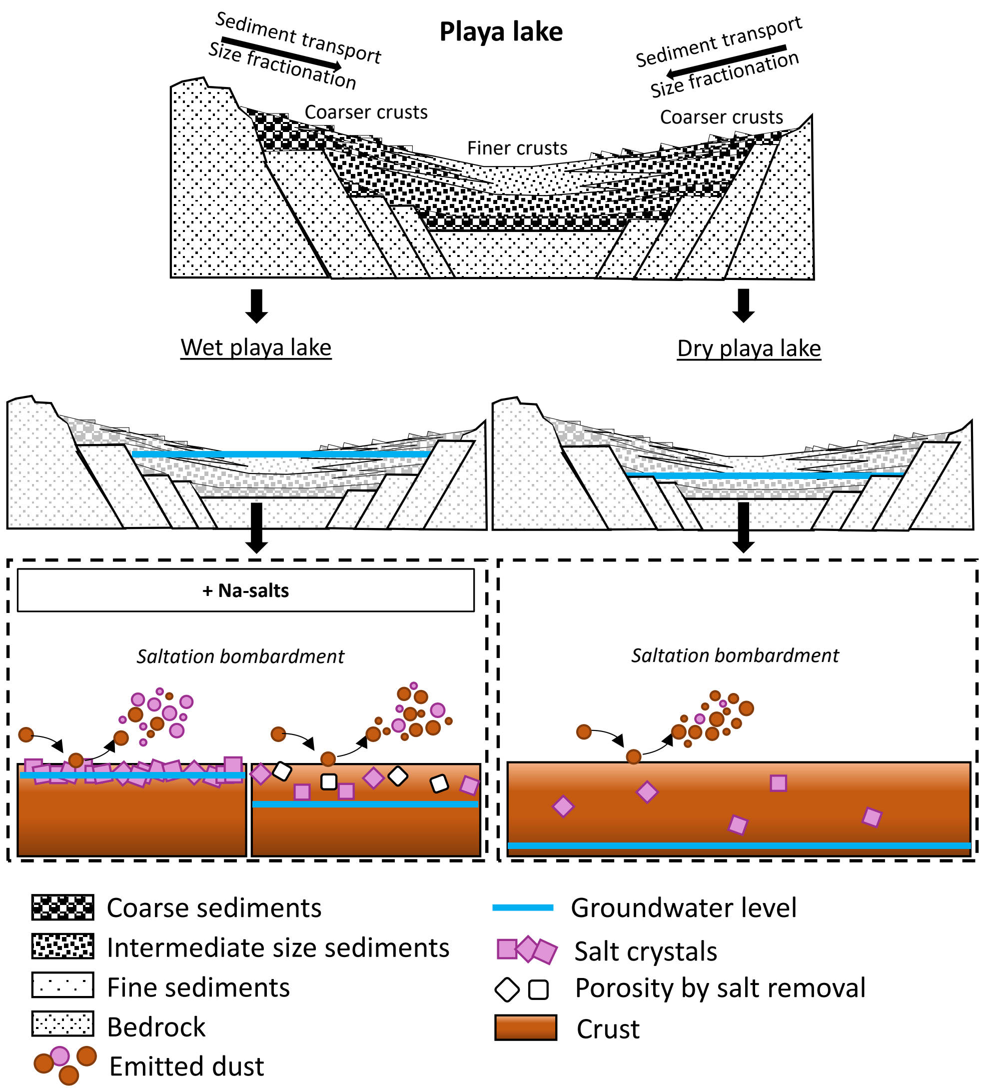

https://doi.org/10.5194/egusphere-2024-434
Preprint. Discussion started: 27 February 2024

Table 1. Full range (<2000 µm), <63µm and >63 to 2000 µm mean diameter, standard deviation, min., and max for minimally dispersed particle size distribution (MDPSD) and fully dispersed particle size distribution (FDPSD).

Surface	Location	N	Full range	≤ 63 µm	>63 to 2000 µm
			MDPSD		
			Mean of medians ± Std. Dev. [Min,Max]		
Crusts	Mojave	35	92 ± 74 [10,349]	22 ± 6.4 [11,34]	254 ± 71 [155,489]
Ripples		20	226 ± 88 [88, 418]	37 ± 6.0 [20,46]	276 ± 80 [130,424]
Crusts	Soda	17	63 ± 47 [10,156]	21 ± 6.5 [11,31]	234 ± 82 [155,489]
	Cronese	9	109 ± 60 [35,195]	18 ± 2.2 [15,22]	280 ± 40 [238,357]
	Mesquite	7	141 ± 117 [31,349]	28 ± 5.6 [21,34]	257 ± 79 [157,387]
	Ivanpah	1	35 ± NA [35,35]	16 ± NA [16,16]	314 ± NA [314,314]
	Coyote	1	101 ± NA [101,101]	20 ± NA [20,20]	254 ± NA [254,254]
Ripples	Soda	15	231 ± 87 [88,418]	39 ± 3.5 [29,43]	275 ± 77 [130,424]
	Cronese	2	264 ± 147 [160,368]	40 ± 8.8 [34,46]	292 ± 120 [208,377]
	Mesquite	2	167 ± 112 [110,225]	26 ± 8.9 [20,32]	286 ± 146 [183,389]
	Ivanpah	0	NA	NA	NA
	Coyote	1	179 ± NA [179,179]	32 ± NA [32,32]	236 ± NA [236,236]
Surface	Location	N	**FDPSD**		
			Full range	≤ 63 µm	>63 to 2000 µm
			Mean of medians ± Std. Dev. [Min,Max]		
Crusts	Mojave	35	37 ± 48 [4.9,240]	18 ± 6.6 [8.4,35]	306 ± 237 [106,1093]
Ripples		20	213 ± 92 [28,362]	29 ± 8.3 [15,48]	335 ± 99 [213,561]
Crusts	Soda	17	52 ± 61 [8.4,240]	19 ± 5.3 [12,27]	321 ± 212 [113,815]
	Cronese	9	17 ± 23 [4.9,77]	12 ± 3.1 [8.4,19]	381 ± 345 [144,1093]
	Mesquite	7	34 ± 28 [11,91]	24 ± 7.7 [16,35]	185 ± 104 [106,336]
	Ivanpah	1	12 ± NA [21,21]	15 ± NA [15,15]	347 ± NA [347,347]
	Coyote	1	8.4 ± NA [8.4,8.4]	12 ± NA [12,12]	187 ± NA [187,187]
Ripples	Soda	15	234 ± 82 [92,362]	31 ± 7.9 [21,48]	346 ± 97 [238,561]
	Cronese	2	236 ± 126 [147,325]	18 ± NA [18,18]	295 ± 108 [219,371]
	Mesquite	2	67 ± 56 [28,107]	27 ± 3.5 [24,29]	336 ± 173 [213,458]
	Ivanpah	0	NA	NA	NA
	Coyote	1	156 ± NA [156,156]	15 ± NA [15,15]	245 ± NA [245,245]

https://doi.org/10.5194/egusphere-2024-434
Preprint. Discussion started: 27 February 2024

Table 2. Average and standard deviations of the mineral contents (wt %) from crust and aeolian ripple samples from the Mojave Desert and the different study basins. NaN, not a number.

	Clays	Carbonate	Salts	Zeolites	Maghemite	Quartz	Feldspars	Gypsum	Amphibole
CRUSTS	24±11	6.6±6.6	7.3±13	1.2±1.9	0.92±0.59	16±7.2	37±9.7	3.1±14	4.1±1.5
Soda	22±11	3.6±2.6	8.9±17	0.77±1.1	0.97±0.66	18±7.7	40±6.7	0.29±0.68	4.5±1.6
Cronese	31±11	5.4±1.8	2.2±3.4	2.4±1.7	1.0±0.28	14±7.3	40±5.5	<0.1	3.4±1.5
Coyote	28	7,2	1,2	8,5	0,48	11	37	<0.1	5.6
Ivanpah	36	6.9	<0.1	<0.1	1,2	15	36	<0.1	3.5
Mesquite	17±8.2	15±11	12±14	<0.1	0.71±0.75	14±5.8	24±12	15±29	2.8±1.4
RIPPLES	7.8±2.3	1.1±2.2	1.1±3,7	0.12±0.52	0.49±0.28	32±9.5	48±13	4.7±20	4.1±1.6
Soda	7.4±1.8	0.47±0.73	0.19±0.46	<0.1	0.49±0.25	35±4.5	52±4.7	<0.1	4.3±1.5
Cronese	8.4±0.60	1.2±1.7	<0.1	<0.1	0.83±0.33	32±9.0	53±0.03	<0.1	4.7±3.2
Coyote	7.9	2.3	<0.1	2,3	0.60	28	52	<0.1	3.5
Ivanpah	NaN	NaN	NaN	NaN	NaN	NaN	NaN	NaN	NaN
Mesquite	10±6.1	4.8±6.8	9.4±9.9	<0.1	0.19±0.27	10±14	15±21	47±60	3.7±1.5

Table 3. Fe content in wt % for total Fe (FeT) content, and in % for ascorbate Fe (FeA), dithionite (FeD), oxalate Fe (FeM) and structural Fe (FeS). NaN not a number.

	FeT	**FeA %**	**FeD %**	**FeM %**	**FeS %**
CRUSTS	3.0±1.3	1.8±0.92	17±7.2	2.1±1.2	79±8.5
Soda	3.1±1.2	1.5±0.81	14±2.5	1.5±0.49	83±2.8
Cronese	3.7±1.2	2.4±0.99	21±11	2.3±1.1	74±13
Coyote	3.5	1.8	14	2.4	82
Ivanpah	4.9	1.4	29	0.82	68
Mesquite	1.6±0.53	1.8±0.93	20±2.7	3.7±1.2	74±3.5
RIPPLES	1.9±1.1	1.4±1.2	12±5.6	2.4±1.8	84±7.5
Soda	2.0±1.2	0.98±0.39	10±3.4	2.1±1.8	87±4.4
Cronese	2.3±1.5	1.4±0.35	14±9.3	2.8±2.9	82±12
Coyote	1.3	3.4	26	3.0	68
Ivanpah	NaN	NaN	NaN	NaN	NaN
Mesquite	1.0±1.1	3.6±3.0	20±1.2	4.4±1.2	73±4.1

https://doi.org/10.5194/egusphere-2024-434
Preprint. Discussion started: 27 February 2024

Table 4. Summarise MDPSD (µm), FDPSD (µm) median particle diameter, Quartz (Qtz, wt %), feldspars (Feld., wt %), clay mineral (Clay, wt %), carbonates (Carb., wt %), Na-salts (Na-S, wt %), Gypsum (Gp, wt %), total Fe content (FeT, wt %), exchangeable Fe (FeA, wt %), dithionite Fe (Hematite and Goethite, wt %), oxalate Fe (FeM, wt %) and structural Fe (FeS, wt %) for Mojave and Morocco crusts and Iceland top sediments. NaN not a number.

	MDPSD d(0.5)	FDPSD d(0.5)	Qtz	Feld.	Clay	Carb.	Na-S	Gp	FeT	FeA	FeD	FeM	FeS
Mojave	92	37	16	37	24	6.6	7.3	3.1	3.0	0.06	0.53	0.06	2.4
Morocco	113	37	48	9.4	17	22	7.0	0.64	3.6	0.07	1.1	NaN	2.4
Iceland	55	56	0.21	20	NaN	NaN	NaN	NaN	9.3	0.15	0.43	1.4	7.3